Supporting Information for "The internal structure and dynamics of Jupiter unveiled by a high resolution magnetic field and secular variation model"

S. Sharan[1], B. Langlais[1], H. Amit[1], E. Thébault[2], M. Pinceloup[1], and O. Verhoeven[1]

[1]Laboratoire de Planétologie et Géosciences, CNRS UMR 6112, Nantes Université, Université d'Angers, Le Mans Université, Nantes, France

[2]Laboratoire Magma et Volcans, Université Clermont Auvergne, UMR 6524, CNRS, IRD, OPGC, Clermont-Ferrand, France

Contents of this file

1. Text S1 and S2
2. Figures S1 to S6

Corresponding authors: S. Sharan, Laboratoire de Planétologie et Géosciences, CNRS UMR 6112, Nantes Université, Université d'Angers, Le Mans Université, Nantes, France (shivangi.sharan@univ-nantes.fr)

Corresponding authors: B. Langlais, Laboratoire de Planétologie et Géosciences, CNRS UMR 6112, Nantes Université, Université d'Angers, Le Mans Université, Nantes, France (benoit.langlais@univ-nantes.fr)

3. Table S1

Text S1. Synthetic simulation

The internal Jovian magnetic field and its temporal rate of change (secular variation) is expanded in terms of Spherical Harmonics (SH). Above the magnetic sources, the vector magnetic field $\overrightarrow{B}$ derives from the expression of a magnetic scalar potential V by $\overrightarrow{B} = -\nabla V$ and where in spherical coordinates it is approximated by the finite series

$$V_{int}(r,\theta,\phi,t) = a \sum_{n=1}^{n_{max}} \sum_{m=0}^{n} \left\{ \left(\frac{a}{r}\right)^{n+1} (g_n^m(t)\cos m\phi + h_n^m(t)\sin m\phi) P_n^m(\cos\theta) \right\} \quad (1)$$

where r denotes the radial distance from the center of Jupiter, a is a reference radius, taken at Jupiter's equatorial radius at 71,492 km, θ is co-latitude, and ϕ the longitude. The functions $P_n^m(\cos\theta)$ are the Schmidt quasi-normalized associated Legendre functions of degree n and order m. The Gauss coefficients g_n^m, h_n^m are the parameters to be estimated by inversion of the measurements. They are functions of time t and are conventionally given in the units of nano-Tesla (nT). The three vector components of Jupiter's magnetic field in the radial, southward and eastward horizontal directions (B_r, B_θ and B_ϕ) are computed taking the negative gradient of Eq. (1).

$$B_r = -\frac{\partial V}{\partial r}, \quad B_\theta = -\frac{1}{r}\frac{\partial V}{\partial \theta}, \quad B_\phi = -\frac{1}{r\sin\theta}\frac{\partial V}{\partial \phi} \quad (2)$$

In order to test the data distribution and its adequacy with model determination, we compute synthetic vector magnetic field values at the actual Juno location and epoch using the Earth CHAOS-7.8 model (Finlay et al., 2020). This time-dependent geomagnetic field is based on magnetic field observations collected by the low-Earth orbit satellites

between years 1999 and 2021. It describes the vector field components up to SH degree $n_{max} = 20$ for the core field with order 6 B-splines (de Boor, 2001) and a 6-month knot separation. The synthetic data therefore contains a significant amount of SV, acceleration, and contributions of higher time derivatives, including some geomagnetic jerks or pulses, which are sudden changes in the second time derivative of the Earth's magnetic field (e.g., Aubert & Finlay, 2019). The full model is used to predict the field over the four years of Juno data.

We test the ability of our algorithm to retrieve the Gauss coefficients of the CHAOS-7.8 model by linear least-squares inversion of the synthetic vector values (Eq. 2) without explicit regularization. We parameterize the inverse problem for the static internal field up to SH degree $n_{max} = 20$. The time resolution of the Gauss coefficients being imposed by Juno's data distribution in time, the temporal variation is restricted to SH degree 8 with a basis of cubic B-splines with 2-yr knot spacing in order to avoid dealing with an ill-conditioned inverse problem. The input and output model parameterizations are thus different, as the synthetic data predicted by the input CHAOS-7.8 is more complex in space and time than what can be recovered by the inverse problem. In order to assess further the robustness of the inversion with respect to noise we test by adding Gaussian random noise of 1 nT to the vector synthetic values.

The assessment of the estimated model can be done by comparisons with the input model in the spatial and/or the spectral domain (see for instance Alken et al. (2021) for a list of possible criteria). Here, our intention being to provide a robust set of Gauss coefficients for the main field and its SV, we show in Figure S4 the comparison between

SH power spectra for the main field and the SV and the SH correlation analysis between the input and the estimated model for these two quantities for the data central epoch.

For this synthetic simulation the estimated coefficients indicate that the main field is well recovered up to SH degree 13 with a degree by degree correlation between coefficients better than 0.8. Beyond the SH degree 14 the power spectrum shows a bell shape structure introduced by spectral leakage and noise amplification. The power spectrum of the SV is in very good agreement with the input model up to SH degree 8 with a correlation better than 0.9. We use these analyses to constrain our field and SV model to degree 13 and 8 respectively.

Text S2. Dynamo Radius Estimate

For Earth, the geomagnetic field spectrum (Lowes, 1966) can be steadily interpreted in terms of magnetic source location. There is an apparent slope break near degree 14 that distinguishes between the energy from the core and crustal field components, respectively. Ignoring the dipole term, the spectrum becomes almost flat when downward extrapolated to the CMB for the core part, while it shows an almost null slope at the surface for higher degrees. This property has been observed for a long time (Lowes, 1974) and has been suggested to provide a crude estimate of the core radius on other planets where seismological measurements are not available.

This crude estimate can be refined by using alternative expressions to the power spectrum. McLeod (1996) defined an expression using magnetic monopoles to estimate core radius. Langlais, Amit, Larnier, Thébault, and Mocquet (2014) defined two additional expressions, first using the non-zonal terms ($m \neq 0$) and the second using the quadrupole

terms ($n+m$ even). These two sub-families show flat spectra independent of degree n at a radius r, interpreted as the CMB for Earth (Figure S5). The non-zonal spectrum has a null slope immediately above the dynamo area. This is expected because the geomagnetic field is axisymmetric on the long term, and the non-axisymmetric part is thought to be random. The flatness of the quadrupole family spectrum is explained by the dominance of rotational effects in the dynamo process. They can be defined as

$$\mathcal{R}_n^{nz}(r) = (n+1)\left(\frac{a}{r}\right)^{(2n+4)} \sum_{m=1}^{n} [(g_n^m)^2 + (h_n^m)^2] \tag{3}$$

$$\mathcal{R}_n^{qf}(r) = (n+1)\left(\frac{a}{r}\right)^{(2n+4)} \sum_{m=0,\ n+m\ even}^{n} [(g_n^m)^2 + (h_n^m)^2] \tag{4}$$

The $\mathcal{R}_n^{nz}$ and $\mathcal{R}_n^{qf}$ provide a more accurate estimate of the radius, much closer to the seismic values, and verified using four different geomagnetic models (Langlais et al., 2014). For CHAOS-4 field model at epoch 2005 and $n = 13$, the R_{nz} is 3,486.6 km and the R_{qf} is 3,496.7 km, which are very close to the accepted seismic value of 3,481.7 km. The values R_{lowes}=3,294.5 km and R_{mcleod}=3,586.5 km are less accurate. The core (or dynamo) radii for other planets were also estimated. Using the JSV model of Ridley and Holme (2016) for Jupiter up to $n = 5$, Langlais et al. (2014) provided the values 0.86 and 0.87 R_J for R_{nz} and R_{qf} respectively. For our model, we estimate the dynamo radius for both the non-zonal and quadrupole family (Figure S6) by varying the truncation degree between 10 and 15, and observe that the radius remains constant up to $n = 13$. The non-zonal spectrum gives a value of 0.851 R_J with a standard deviation of 0.012 R_J, while the quadrupole family spectrum returns 0.839 R_J with a standard deviation of 0.018 R_J. The mean of the radii estimated using $n_{max} = 13$ corresponds to 0.845±0.015 R_J.

References

Alken, P., Thébault, E., Beggan, C. D., Aubert, J., Baerenzung, J., Brown, W. J., ... Wardinski, I. (2021). Evaluation of candidate models for the 13th generation international geomagnetic reference field. *Earth, Planets and Space*, *73*(1), 48. Retrieved from https://doi.org/10.1186/s40623-020-01281-4 doi: 10.1186/s40623-020-01281-4

Aubert, J., & Finlay, C. C. (2019). Geomagnetic jerks and rapid hydromagnetic waves focusing at earth's core surface. *Nature Geoscience*, *12*(5), 393–398. Retrieved from https://doi.org/10.1038/s41561-019-0355-1 doi: 10.1038/s41561-019-0355-1

Connerney, J. E. P., Kotsiaros, S., Oliversen, R. J., Espley, J. R., Joergensen, J. L., Joergensen, P. S., ... Levin, S. M. (2018). A new model of jupiter's magnetic field from juno's first nine orbits. *Geophysical Research Letters*, *45*(6), 2590-2596. Retrieved from https://agupubs.onlinelibrary.wiley.com/doi/abs/10.1002/2018GL077312 doi: https://doi.org/10.1002/2018GL077312

de Boor, C. (2001). Calculation of the smoothing spline with weighted roughness measure. *Mathematical Models and Methods in Applied Sciences*, *11*(01), 33-41. Retrieved from https://doi.org/10.1142/S0218202501000726 doi: 10.1142/S0218202501000726

Finlay, C. C., Kloss, C., Olsen, N., Hammer, M. D., Tøffner-Clausen, L., Grayver, A., & Kuvshinov, A. (2020). The chaos-7 geomagnetic field model and observed changes in the south atlantic anomaly. *Earth, Planets and Space*, *72*(1), 156. Retrieved from https://doi.org/10.1186/s40623-020-01252-9 doi: 10.1186/s40623-020-01252

-9

Langlais, B., Amit, H., Larnier, H., Thébault, E., & Mocquet, A. (2014). A new model for the (geo)magnetic power spectrum, with application to planetary dynamo radii. *Earth and Planetary Science Letters*, *401*, 347-358. Retrieved from https://www.sciencedirect.com/science/article/pii/S0012821X14003070 doi: https://doi.org/10.1016/j.epsl.2014.05.013

Lowes, F. J. (1966). Mean-square values on sphere of spherical harmonic vector fields. *Journal of Geophysical Research (1896-1977)*, *71*(8), 2179-2179. Retrieved from https://agupubs.onlinelibrary.wiley.com/doi/abs/10.1029/JZ071i008p02179 doi: https://doi.org/10.1029/JZ071i008p02179

Lowes, F. J. (1974, 03). Spatial power spectrum of the main geomagnetic field, and extrapolation to the core. *Geophysical Journal International*, *36*(3), 717-730. Retrieved from https://doi.org/10.1111/j.1365-246X.1974.tb00622.x doi: 10.1111/j.1365-246X.1974.tb00622.x

McLeod, M. G. (1996). Spatial and temporal power spectra of the geomagnetic field. *Journal of Geophysical Research: Solid Earth*, *101*(B2), 2745-2763. Retrieved from https://agupubs.onlinelibrary.wiley.com/doi/abs/10.1029/95JB03042 doi: https://doi.org/10.1029/95JB03042

Ridley, V. A., & Holme, R. (2016). Modeling the jovian magnetic field and its secular variation using all available magnetic field observations. *Journal of Geophysical Research: Planets*, *121*(3), 309-337. Retrieved from https://agupubs.onlinelibrary.wiley.com/doi/abs/10.1002/2015JE004951 doi: https://doi

.org/10.1002/2015JE004951

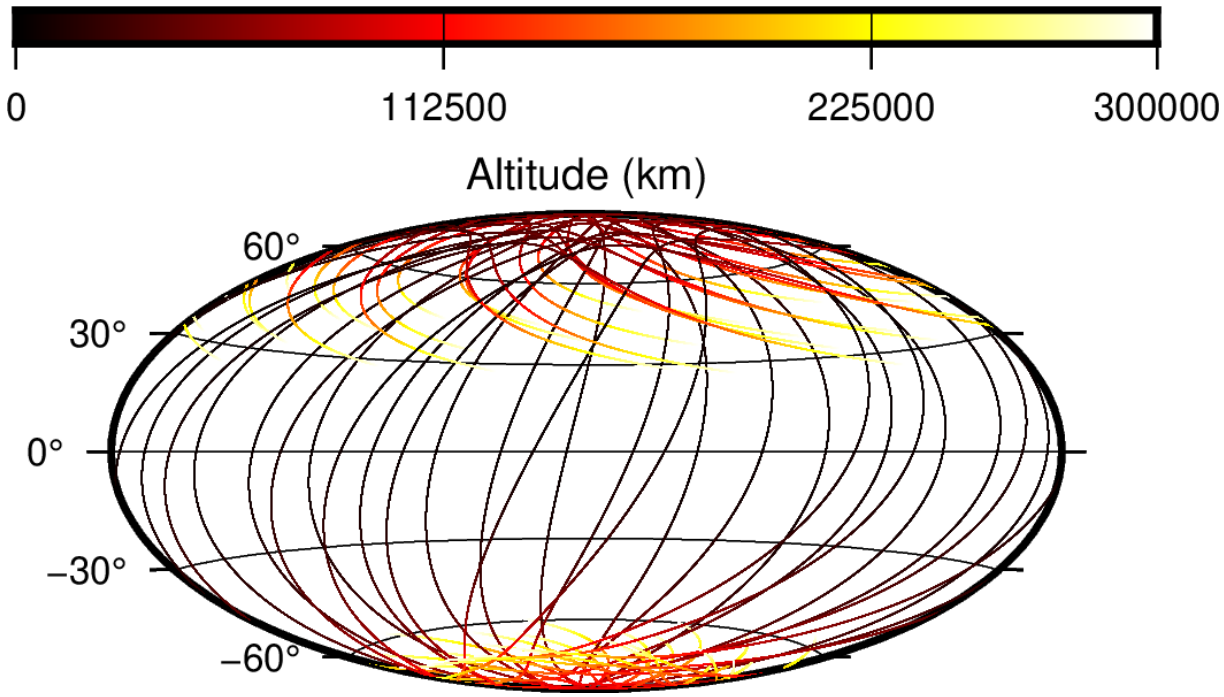

Figure S1. The data locations of Juno satellite below 300,000 km for the first 28 (without orbit 2 and 19) perijoves. The colours represent different altitudes above the surface.

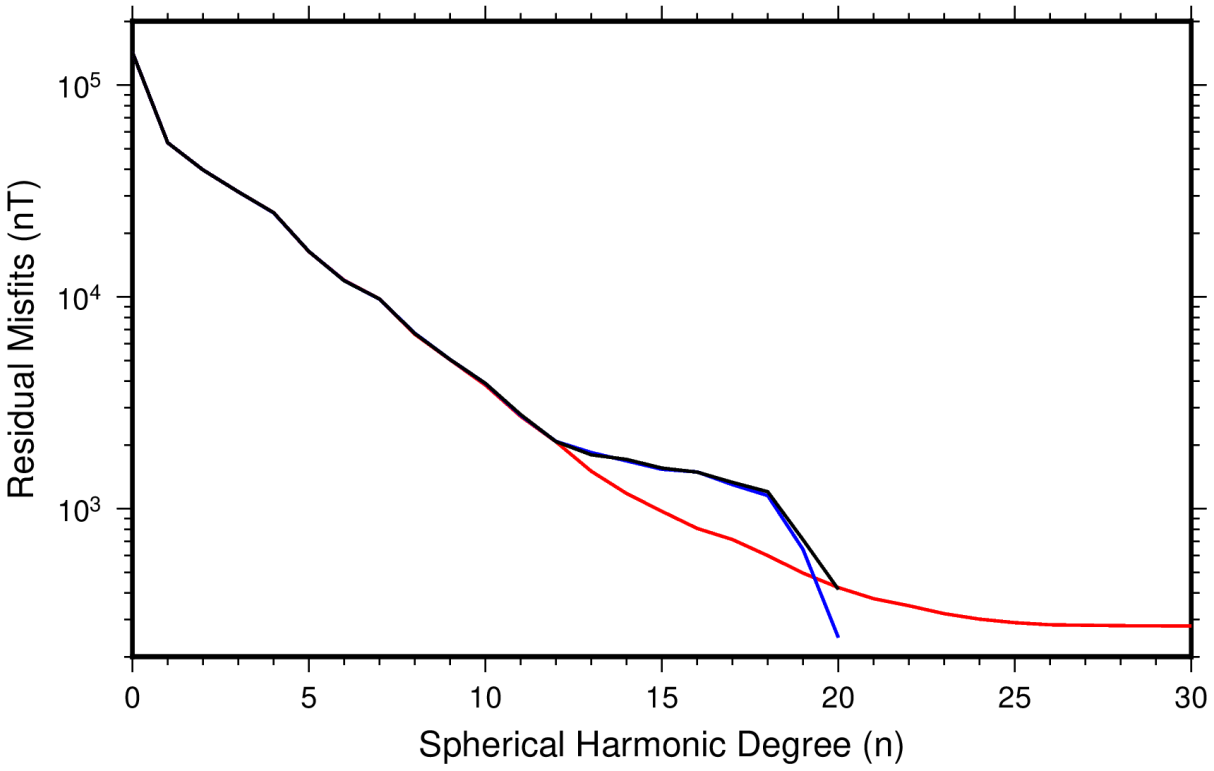

Figure S2. The residual misfits plotted as a function of the SH degree for the model by Connerney et al. (2018) (red), a model without SV (blue) and our model (black).

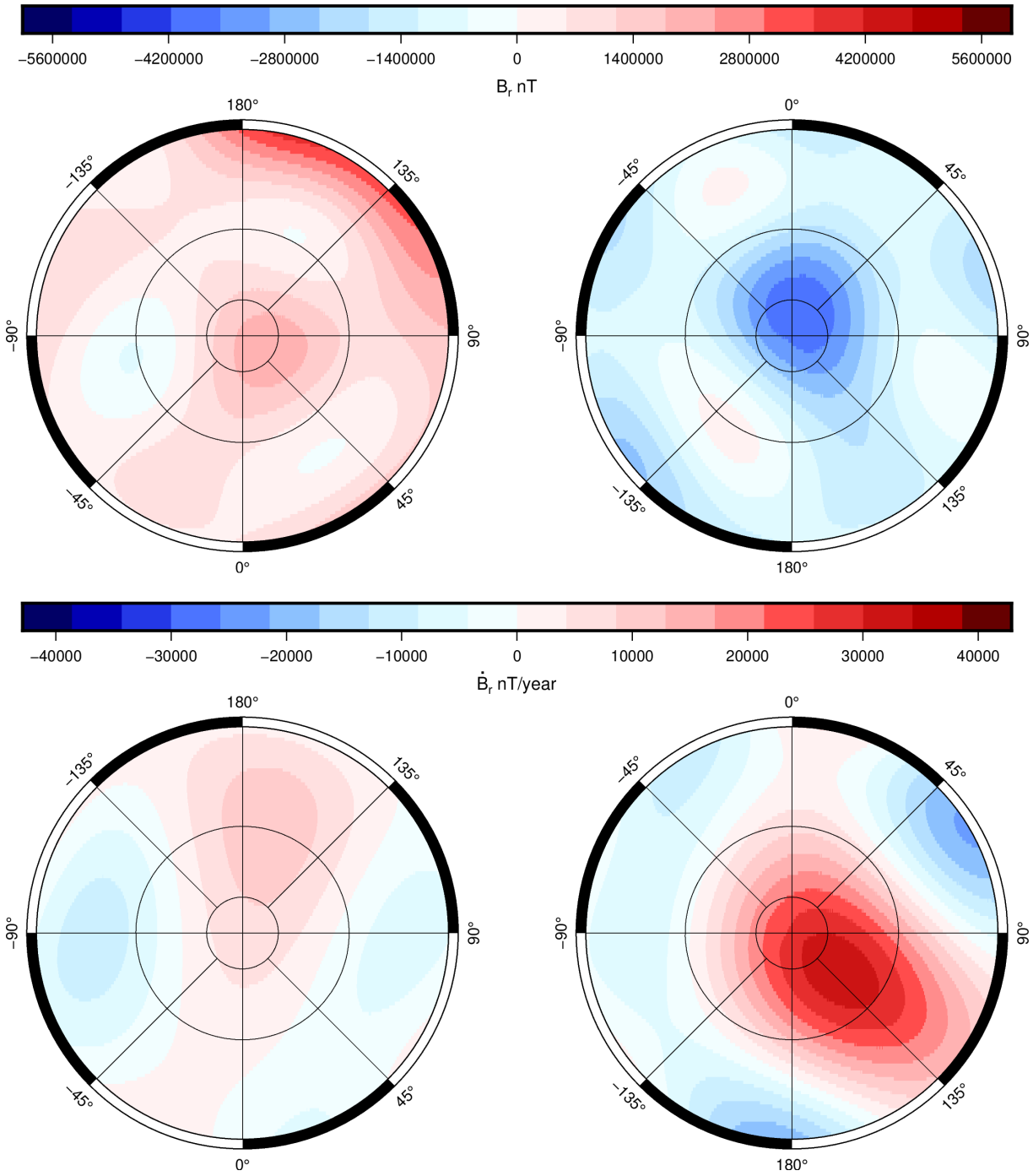

Figure S3. The (top) radial field and (bottom) radial secular variation at $\mathbf{R}_{sf}$ for the (left) North Pole and (right) South Pole. The inner to outer circles represent latitudes 85°, 75° and 60° respectively.

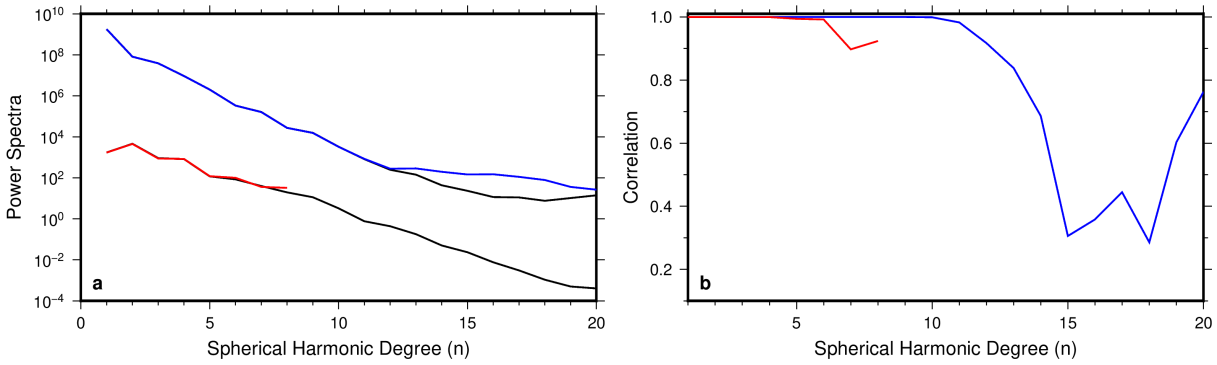

Figure S4. (**a**) The power spectrum of the main field (shown in blue, units - nT^2) and secular variation (shown in red, units - $(nT/year)^2$) of the estimated and input (black) geomagnetic model. (**b**) The correlation between the estimated and input model for the main field (blue) and SV (red).

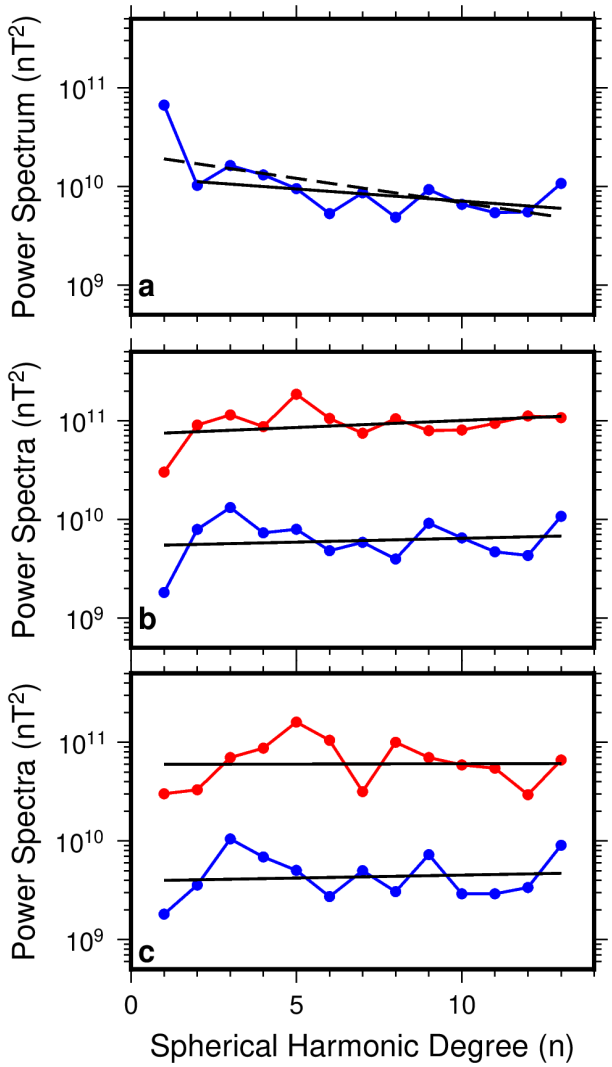

Figure S5. (**a**) Geomagnetic power spectrum of CHAOS-7.8 model at the CMB with linear regression from n=1-13 (black dashed line, slope = -0.0493) and 2-13 (black line, slope = -0.0245). (**b**) The non-zonal spectra with linear regression (black line) for the geomagnetic model (blue, slope = 0.0077) at CMB and for our model (red, slope = 0.0142) at $\mathbf{R}_{sf}$. (**c**) The quadrupole family spectra with linear regression (black line) for the geomagnetic field (blue, slope = 0.0060) at CMB and for our model (red, slope = 0.0007) at $\mathbf{R}_{sf}$.

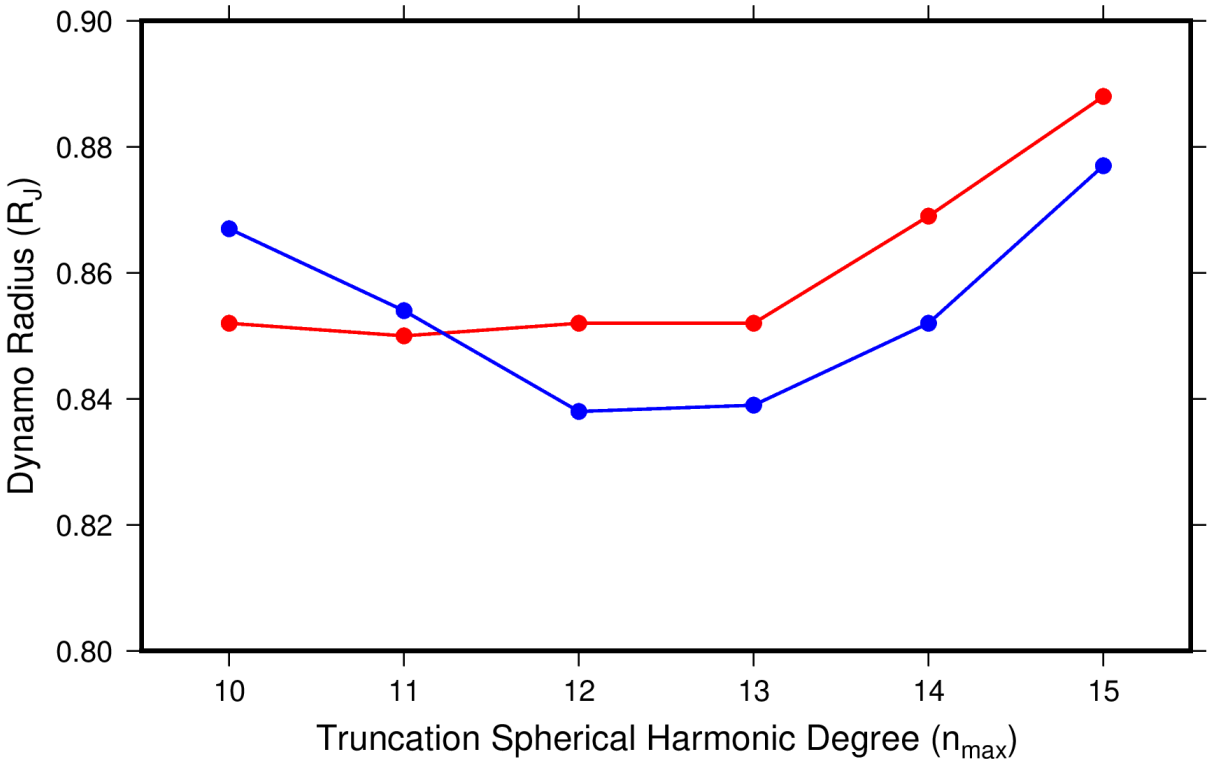

Figure S6. The dynamo radius calculated using the non-zonal (red) and quadrupole (blue) terms for different truncation degrees.

Table S1. Misfits (in nT) without and with secular variation.

	B_r	B_θ	B_ϕ	**B**
model without SV	1982	1768	796	1843
model with SV	1948	1706	810	1796